JOC Article

Total *carbo*-Mer of Benzene, Its *carbo*-Trannulene Form, and the Zigzag Nanotube Thereof

Christine Lepetit, Chunhai Zou, and Remi Chauvin*

Laboratoire de Chimie de Coordination, UPR 8241 CNRS, 205 Route de Narbonne, 31 077 Toulouse Cedex 4, France

chauvin@lcc-toulouse.fr

Received December 12, 2005

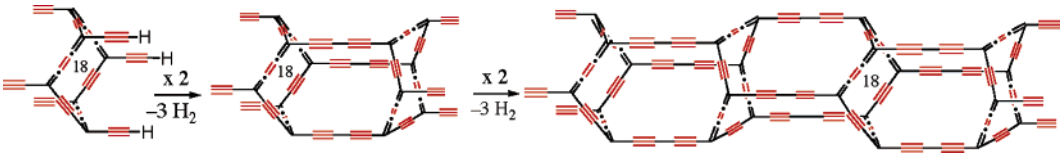

The total *carbo*-mer of benzene, hexaethynyl *carbo*-benzene $C_{30}H_6$, has been calculated at the B3PW91/6-31G** level. Its geometrical and magnetic characteristics are compared with those of the $C_{18}H_6$ partial *carbo*-mers, unsubstituted *carbo*-benzene, and hexaethynylbenzene. The *carbo*-[6]trannulene isomer is found to exist as a minimum on the singlet spin state potential energy surface (PES) and is 65.6 kcal·mol^{-1} higher in energy than hexaethynyl-*carbo*-benzene. In the former, a strong cyclic electron delocalization is evidenced from the root-mean-square deviation (rms) of the ring bond lengths and the NICS value computed at the centroid of the trannulene ring. As an alternative to the graphene sheet wrapping process traditionally used to illustrate the construction of carbon nanotubes, a dehydrocoupling-stacking process is invoked for the construction of zigzag nanotubes from trannulene bricks. The process is applied to the *carbo*-[6]trannulene brick to generate a novel type of acetylene-expanded carbon nanotube, which is a polymer of primitive C_{60} segments. A $C_{60}H_6$ *carbo*-meric equivalent of a cyclacene belt is first considered. Two such segments are then formally dehydrocoupled to generate a cylindrical $(C_{60})_2H_6$ molecule, the central part of which is assumed to be a relevant model for the infinite nanotube. Axial and sectional electron delocalization inside the tube models is discussed on the basis of bond length analysis, NICS values, π MO analysis, and singlet−triplet state energy gap. The capping of the C_{120} cyclinder is finally addressed by use of *carbo*-[3]radialenic units.

Introduction

The early definition of *carbo*-meric molecules was illustrated for benzene.[1] It was proposed that the *carbo*-merization process can apply to any subset of symmetry-related bonds in the molecule:[2] the six peripheral C−H bonds, the six C−C bonds of the ring, or both, namely, the twelve bonds of benzene.

The peripheral *carbo*-mer of benzene **1** (Scheme 1) is actually hexaethynylbenzene, an experimentally known molecule that was also studied at various theoretical levels.[3,4]

The ring *carbo*-mer of benzene **2** (Scheme 1) is still unknown,[5,6] but several aryl-substituted derivatives have been experimentally described.[7] Nevertheless, the unsubstituted $C_{18}H_6$ molecule **2**[8] was calculated at the DFT level, and it was shown to be definitely aromatic in the structural, magnetic, and energetic sense.[9] Properties related to the presence and the aromaticity of the *carbo*-benzene ring such as hyperpolarizability were also investigated.[10]

* To whom correspondence should be addressed. Phone: 33 (0)5 61 33 31 13.

(1) Chauvin, R. *Tetrahedron Lett.* **1995**, *36*, 397.

(2) Partial *carbo*-mers of any given molecule, even of C_1 symmetry, are therefore ethynylogues or second cumulogues thereof.

(3) (a) Diercks, R.; Armstrong, J. C.: Boese, R.; Vollhardt, K. P. C. *Angew. Chem., Int. Ed. Engl.* **1986**, *25*, 268. (b) El-Shall, M. S.; Vollhardt, K. P. C. *J. Mol. Struct. (THEOCHEM)* **1989**, *183*, 175. (c) Fowler, P. W.; Steiner, E.; Zanasi, R.; Cadioli, B. *Mol. Phys.* **1999**, *96*, 1099.

(4) Yavari, I.; Jabbari, A.; Samadizadeh, M. *J. Chem. Res., Synop.* **1999**, 152.

(5) For the sake of simplicity, the ring *carbo*-mer of benzene has been called "*carbo*-benzene" instead of its first proposed nomenclature [C,C]$_6$ *carbo*-benzene.

(6) Chauvin, R. *Tetrahedron Lett.* **1995**, *36*, 401.

(7) (a) Kuwatani, Y.; Watanabe, N.; Ueda, I. *Tetrahedron Lett.* **1995**, *36*, 119. (b) Suzuki, R.; Tsukude, H.; Watanabe, N.; Kuwatani, Y.; Ueda, I. *Tetrahedron* **1998**, *54*, 2477. (c) Maurette, L. Ph.D. dissertation, Université Paul Sabatier, Toulouse, 2002. (d) Saccavini, C. Ph.D. dissertation, Université Paul Sabatier, Toulouse, 2004.

(8) Chauvin, R.; Lepetit, C. *Acetylene Chemistry. Chemistry, Biology and Material Sciences*; Diederich, F., Stang, P. J., Tykwinski R. R., Eds.; Wiley: Weinheim, 2005; Chapter1, p 1.

10.1021/jo052551j CCC: $33.50
Published on Web 07/18/2006

SCHEME 1. Molecular Structures Studied: Peripheral *carbo*-Mer of Benzene (1), Ring *carbo*-Mer of Benzene Referred to as *carbo*-Benzene for Convenience (2), Total *carbo*-Mer of Benzene (or hexaethynyl-*carbo*-benzene) (3), and Its *carbo*-[6]Trannulene Isomer (4)

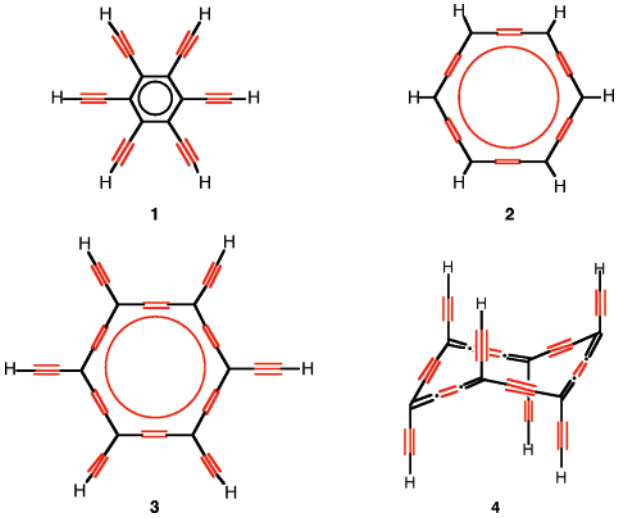

Since it has been first mentioned in 1995,[1] the total *carbo*-mer of benzene **3** (Scheme 1) ($C_{30}H_6$, hexaethynyl- "*carbo*-benzene") has not been studied. The preliminary part of this work intends to fill this gap. A triethylsilyl derivative of **3** has been recently obtained experimentally.[11] These new experimental results prompted us to pursue and extend theoretical investigations toward possible implication of **3** in the design of novel carbon materials; the results are presented in a second section.

Computational Details

Geometries were fully optimized (under symmetry constraint whenever possible) at the BP86/6-31G** and B3PW91/6-31G** levels using Gaussian98[12] or Gaussian03[13] in the singlet spin state. Although DFT methods have been reported to overestimate electron delocalization in polyyne/cumulene systems,[14] the B3PW91/6-31G** level of calculation proved to be suitable to describe the geometry and NMR properties of substituted *carbo*-benzenes. At this level, indeed, calculated geometries are in very good agreement with the available experimental crystallographic structures.[8,15] For compound **5A**, PW91PW91/6-31G** and B3LYP/6-31G** calculations afforded essentially the same geometry and electronic structures as did BP86/6-31G** and B3PW91/6-31G** calculations, respectively (see Table S1 of Supporting Information). Triplet spin states were calculated at the UB3PW91/6-31G** level as no spin contamination was observed (S**2 $\approx$ 2.05). The stability of the wave function was checked. [9]Cyclacene, from which (9,0) nanotubes are built (Scheme 2), was recently shown to be better described as an open shell singlet.[16] This is however not the case for the present nanotube models **4**−**7** (vide infra). The wave functions of models **4**−**7** were indeed unstable at the restricted level. However, re-optimization using the unrestricted broken symmetry UB3PW91/6-31G** level (even when the symmetry of the wave function is shut off explicitly using the symm=noscf keyword) yielded the same geometries and almost the same total energies as for the corresponding closed shell singlets. The broken spin unstability might be ascribed to the proximity of the triplet spin state. Vibrational analysis was performed at the same level in order to check that a minimum was obtained on the potential energy surface. For compounds **6** and **7**, however, it was not possible to achieve the vibrational analysis within the maximum allowed CPU time. BP86/6-31G** calculations were used as first guesses for hybrid DFT calculations. The corresponding geometries exhibit longer C_2 units and are thus indicative of a slightly more pronounced electron delocalization. Only the higher level B3PW91/6-31G** or B3PW91/6-311+G** geometries are discussed hereafter.

NICS (nucleus independent chemical shifts) were computed according to the procedure described by Schleyer et al.[17] The magnetic shielding tensor was calculated for a ghost atom located at the geometric center of the ring or 1 Å above this center, using the GIAO (gauge-independent atomic orbital) method implemented in Gaussian03.[13]

Results and Discussion

Hexaethynyl-*carbo*-Benzene, the Total *carbo*-Mer of Benzene. At the B3PW91/6-31G** level, a planar D_{6h} structure is calculated for **3** (Figure 1a). The ring bond lengths are close to those found in the partial ring *carbo*-mer **2**, while the peripheral triple bonds exhibit classical lengths for terminal alkynes (Table 1). Let $\sigma_r(d)$ and $\sigma_s(d)$ denote the root-mean-square deviations (rms in Å) from the mean C−C bond length over the C_{18} ring and over the C_{30} whole skeleton, respectively. The $\sigma_r(d)$ values

(9) (a) Godard, C.; Lepetit, C.; Chauvin, R. *Chem. Commun.* **2000**, 1833. (b) Lepetit, C.; Godard, C.; Chauvin, R. *New. J. Chem.* **2001**, *25*, 572. (c) Lepetit, C.; Silvi, B.; Chauvin, R. *J. Phys. Chem. A* **2003**, *107*, 464. (d) Lepetit, C.; Peyrou, V.; Chauvin, R. *Phys. Chem. Chem. Phys.* **2004**, *6*, 303.

(10) (a) Ducere, J.-M.; Lepetit, C.; Lacroix, P. G.; Heully, J.-L.; Chauvin, R. *Chem. Mater.* **2002**, *14*, 3332. (b) Lepetit, C.; Lacroix, P. G.; Peyrou, V.; Saccavini, C.; Chauvin, R. *J. Comput. Methods Sci. Eng.* **2004**, *4* (3−4), 569.

(11) Zou, C.; Chauvin, R. Unpublished results.

(12) Frisch, M. J.; Trucks, G. W.; Schlegel, H. B.; Scuseria, G. E.; Robb, M. A.; Cheeseman, J. R.; Zakrzewski, V. G.; Montgomery, J. A., Jr., Stratmann, R. E.; Burant, J. C.; Dapprich, S.; Millam, J. M.; Daniels, A. D.; Kudin, K. N.; Strain, M. C.; Farkas, O.; Tomasi, J.; Barone, V.; Cossi, M.; Cammi, R.; Mennucci, B.; Pomelli, C.; Adamo, C.; Clifford, S.; Ochterski, J.; Petersson, G. A.; Ayala, P. Y.; Cui, Q.; Morokuma, K.; Malick, D. K.; Rabuck, A. D.; Raghavachari, K.; Foresman, J. B.; Cioslowski, J.; Ortiz, J. V.; Baboul, A. G.; Stefanov, B. B.; Liu, G.; Liashenko, A.; Piskorz, P.; Komaromi, I.; Gomperts, R.; Martin, R. L.; Fox, D. J.; Keith, T.; Al-Laham, M. A.; Peng, C. Y.; Nanayakkara, A.; Gonzalez, C.; Challacombe, M.; Gill, P. M. W.; Johnson, B.; Chen, W.; Wong, M. W.; Andres, J. L.; Gonzalez, C.; Head-Gordon, M.; Replogle, E. S.; Pople, J. A., *Gaussian 98*, Revision A.7; Gaussian, Inc.: Pittsburgh, PA, 1998.

(13) Frisch, M. J.; Trucks, G. W.; Schlegel, H. B.; Scuseria, G. E.; Robb, M. A.; Cheeseman, J. R.; Montgomery, J. A., Jr.; Vreven, T.; Kudin, K. N.; Burant, J. C.; Millam, J. M.; Iyengar, S. S. Tomasi, J.; Barone, V.; Mennucci, B.; Cossi, M.; Scalmani, G.; Rega, N.; Petersson, G. A.; Nakatsuji, H.; Hada, M.; Ehara, M.; Toyota, K.; Fukuda, R.; Hasegawa, J.; Ishida, M.; Nakajima, T.; Honda, Y.; Kitao, O.; Nakai, H.; Klene, M.; Li, X.; Knox, J. E.; Hratchian, H. P.; Cross, J. B.; Adamo, C.; Jaramillo, J.; Gomperts, R.; Stratmann, R. E.; Yazyev, O.; Austin, A. J.; Cammi, R.; Pomelli, C.; Ochterski, J. W.; Ayala, P. Y.; Morokuma, K.; Voth, G. A.; Salvador, P.; Dannenberg, J. J.; Zakrzewski, V. G.; Dapprich, S.; Daniels, A. D.; Strain, M. C.; Farkas, O.; Malick, D. K.; Rabuck, A. D.; Raghavachari, K.; Foresman, J. B.; Ortiz, J. V.; Cui, Q.; Baboul, A. G.; Clifford, S.; Cioslowski, J.; Stefanov, B. B.; Liu, G.; Liashenko, A.; Piskorz, P.; Komaromi, I.; Martin, R. L.; Fox, D. J.; Keith, T.; Al-Laham, M. A.; Peng, C. Y.; Nanayakkara, A.; Challacombe, M.; Gill, P. M. W.; Johnson, B. W.; Wong, W.; Gonzalez, C. and Pople, J. A., *Gaussian 03*, Revision B.05; Gaussian, Inc.: Pittsburgh, PA, 2003.

(14) (a) Plattner, D. A.; Houk, K. N. *J. Am. Chem. Soc.* **1995**, *117*, 4405. (b) Pomerantz, A. E.; Han, J. H.; Musgrave, C. B. *J. Phys. Chem. A* **2004**, *108*, 4030.

(15) Zou, C.; Lepetit, C.; Coppel, Y.; Chauvin, R. *Pure Appl. Chem.* **2006**, *78*, 791.

(16) (a) Bendikov, M.; Duong, H. M.; Starkey, K.; Houk, K. N.; Carter, E. A.; Wudl, F. *J. Am. Chem. Soc.* **2004**, *126*, 7416. (b) Poater, J.; Bofill, J. M.; Alemany, P.; Sola, M. *J. Phys. Chem.* A **2005**, *109*, 10629. (c) Portella, G.; Poater, J.; Bofill, J. M.; Alemany, P.; Sola, M. *J. Org. Chem.* **2005**, *70*, 2509.

(17) Schleyer, P. v. R.; Maerker, C.; Dransfeld, A.; Jiao, H.; Hommes, N. J. R. v. E. *J. Am. Chem. Soc.*, **1996**, *118*, 6317.

SCHEME 2. Construction of Zigzag Nanotubes with C_{18} Sectional Rings through Formal Dehydrocoupling Processes ("Stacking" Approach)[a]

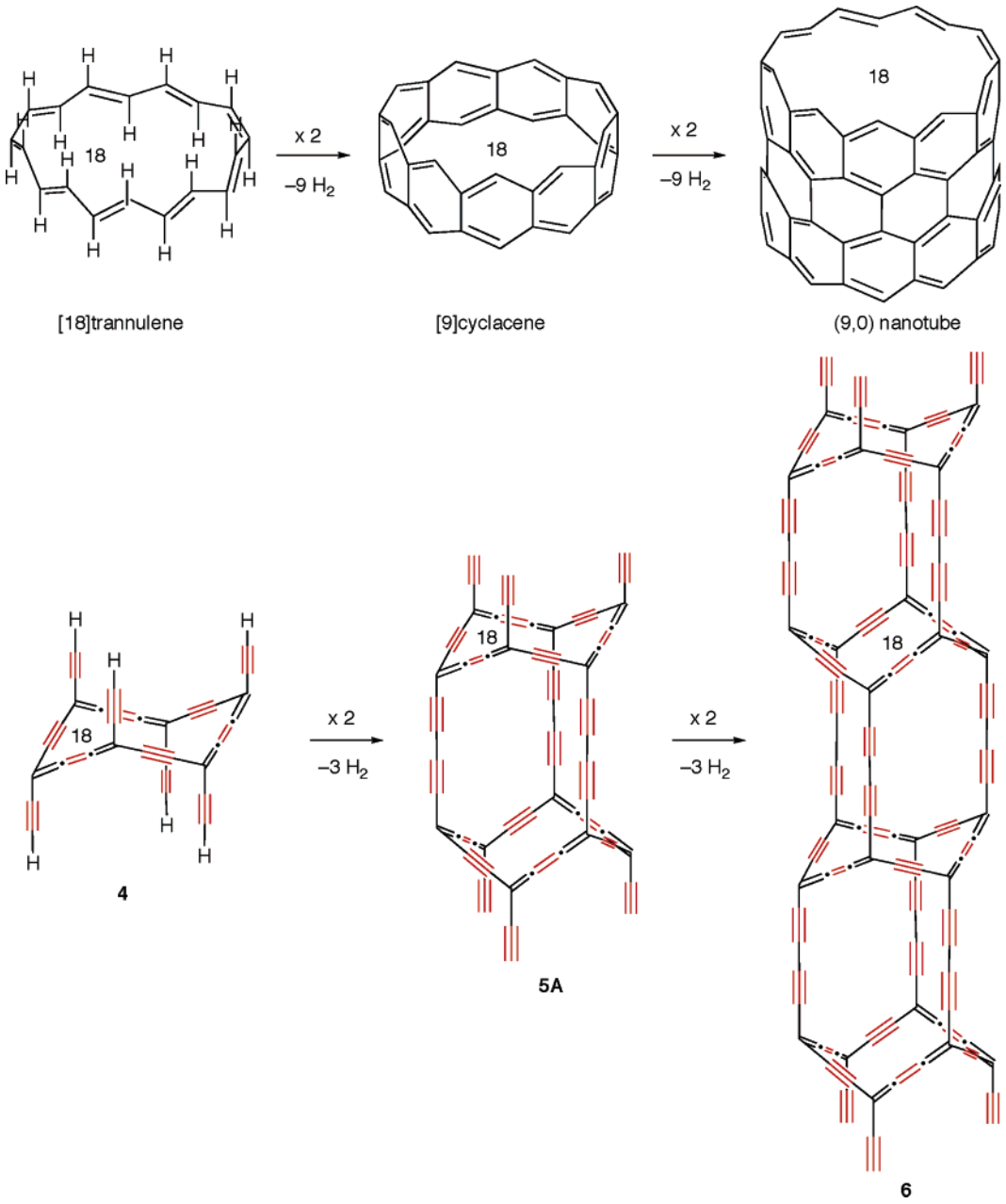

[a] Whereas the (9,0) nanotube is built from [18]trannulene, the nanotube model **6** is built from hexaethynyl-*carbo*-[6]trannulene **4**. After the first step, one obtains the elementary unit having the same symmetry as the infinite tube, namely, the [9]cyclacene and the $C_{60}H_6$ cage molecule **5A** for the (9,0) nanotube and the nanotube model **6**, respectively.

indicate that the endocyclic electron delocalization in **3** is lower ($\sigma_r(d) = 0.070$ Å) than in the unsubstituted version **2** ($\sigma_r(d) = 0.061$ Å). At the B3PW91/6-311+G** level, the C−C bonds of **3** are all shortened, but the $\sigma_r(d)$ and $\sigma_s(d)$ values remain the same (Table 1). Although $\sigma_r(d)$ values can be directly analyzed in terms of the variation of endocyclic hybridization states and thus depend on the ring substitution, they are also indicators of electron delocalization. $\sigma_r(d)$ is indeed proportional to Krygowski's GEO parameter, the geometric component of the HOMA aromaticity index.[18] The $\sigma_r(d)$ values of Table 1 are qualitatively consistent with the corresponding NICS values.

At the HF/6-31+G** level, the NICS value calculated at the geometric center of the ring (NICS(0)) is close to the value calculated 1 Å above the ring(NICS(1)) (Table 1). The NICS value thus seems to not markedly vary with distance. This is in contrast with Stanger's recent finding that NICS variation versus distance is a discriminating indicator of the magnetic aromaticity of small simple π-systems.[19] Although the variation of dissected NICS components (in-plane vs out-of-plane) could deserve more detailed investigations, our two-point data on isotropic NICS complement Stanger's analysis for extended double π-systems. Moreoever, Schleyer recently showed that despite some imperfections, isotropic NICS(0) is a reliable qualitative indicator of magnetic aromaticity, which can be only *refined* by the

(18) Krygowski, T. M.; Cyrañski, M. K. *Chem. Rev.* **2001**, *101*, 1395.

TABLE 1. Structural and Magnetic Properties of Benzene and [6]Trannulene *carbo*-Mers at the B3PW91/6-31G Level[a]**

	ring[a]					periph[a]				
	sp-sp^2-sp	sp^2-sp-sp	sp-sp	sp-sp^2	σ_r(d)[b]	sp-sp	sp-sp^2	σ_s(d)[c]	symmetry	NICS(0) [NICS(1)][d]
benzene	120°		1.394		0			0	D_{6h}	−9.7
1	120°		1.414		0	1.210	1.421	0.098	D_{6h}	−11.0 [−11.0]
2	122.6°	178.7°	1.239	1.369	0.061			0.061	D_{6h}	−19.7 [−18.0]
3[e]	120.3°	179.8°	1.233	1.382	0.070	1.211	1.424	0.087	D_{6h}	−17.8 [−16.3]
	(120.5°)	(179.8°)	(1.228)	(1.378)	(0.071)	(1.206)	(1.422)	(0.088)	(D_{6h})	(−17.8)[f]
4	118.5°	160.4°	1.238	1.387	0.070	1.212	1.421	0.086	D_{3d}	−15.3 [−13.3]

[a] Bond lengths are in Å . [b] $\sigma_r(d) = \{1/N \sum(d_i - \langle d\rangle)^2\}^{1/2}$, where N is the number of C−C bonds in the ring (6 or 18), d_i denotes the length of the ith C−C bond in the ring, and $\langle d\rangle$ is the mean bond length in the ring. [c] $\sigma_s(d) = \{1/N' \sum(d_i - \langle d\rangle)^2\}^{1/2}$, where N' is the total number of C−C bonds (6, 12, 18 or 30), d_i denotes the length of the ith C−C bond, and $\langle d\rangle$ is the mean bond length. [d] In ppm units. NICS were calculated at the geometric center of the rings (NICS(0)) or 1 Å above this geometric center (NICS(1)), within the framework of the GIAO formalism at the HF/6-31+G*//B3PW91/6-31G** level. [e] Values calculated at the B3PW91/6-311+G** level are in parentheses. [f] HF/6-31+G*//B3PW91/6-311+G** level.

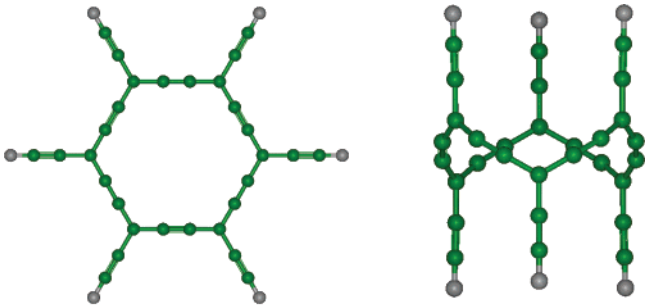

FIGURE 1. Optimized geometry in the singlet spin state at the B3PW91/6-31G** level of (a) the total *carbo*-mer of benzene **3**, and (b) its *carbo*-trannulenic isomer **4**.

consideration of other dissected and/or remote NICS parameters.[20] Negative NICS(0) and NICS(1) values can therefore be confidently considered as revealing the diamagnetic character of **2** and other molecules in Table 1. The NICS(0) value of **3** is slightly less negative (−17.8 ppm) than the corresponding value for **2** (−19.7 ppm). By contrast to what was observed in the isomeric neutral *carbo*-radialenic series,[21] the ethynyl substitution of the C_{18} ring decreases the magnetic aromaticity. Similarly to the former series, the ethynyl substitution of the benzene ring increases the magnetic aromaticity in the resulting hexaethynylbenzene (**1**) (Table 1).

Both the NICS and σ_r(d) relative values tend to show that hexaethynyl-*carbo*-benzene **3** tends to be less aromatic than its unsubstituted congener **2**, at least in the magnetic and structural sense. It may be again stressed that σ_r(d) values are also influenced by the degree of substitution of the ring.

Hexaethynyl *carbo*-[6]Trannulene. Owing its large ring size (C_{18}), the possibility of a nonplanar isomer of **3** could not be ruled out a priori. Indeed, the all-*trans* isomers of large planar annulenes have been considered as viable structures and referred to as "[*n*]trannulenes".[22] Just as their [*n*]annulene isomers (containing *cis* double bonds), these molecules are cyclically conjugated, but contrary to the former, which exhibit out-of-plane π-overlap of n p_z atomic orbitals (AOs), [*n*]trannulenes exhibit in-plane π-ovelap of n p_{xy} AOs (the z axes are taken as perpendicular to the mean ring planes). Although [*n*]trannulenes and in particular [18]trannulene are kinetically instable unless embedded into fullerene cages,[23,24] the unstrained trannulenes C_nH_n were systematically studied by Schleyer et al. at the DFT level for $n \geq 10$.[22] The trannulenic form of benzene ($n = 6$), namely *trans*,*trans*,*trans*-cyclohexatriene, does not exist, but what about its *carbo*-mer, which contains a 18-membered ring? Beyond the strict application of VSEPR, the angular strain could be indeed diluted out over the whole ring, and efficiently relieved by the sp carbon atoms. The trannulene stereoisomer (**4**) of the total *carbo*-mer of benzene (Scheme 1) thus deserved to be investigated.

At the B3PW91/6-31G** level, a trannulene-like ("*carbo*-trannulenic") minimum **4** of D_{3d} symmetry was indeed found on the singlet spin state potential energy surface (PES), 65.6 kcal·mol^{-1} above the D_{6h} minimum **3** (Figure 1b). The conversion barrier of **4** to **3** was estimated to be ca. 9 kcal·mol^{-1} (Figure S1). The corresponding IRC (intrinsic reaction coordinate) shows that **4** does not lie in a very deep well.

Astonishingly, the bond lengths in the *carbo*-trannulenic molecule **4** are very similar to those occurring in the *carbo*-annulenic isomer **3**. In particular, the σ_r(d) and σ_s(d) values are identical in both the trannulenic and annulenic forms: the endocyclic and overall electron delocalization are maintained at the same level through either out-of-plane or in-plane π-overlap. By contrast, the NICS values are indicative of a lower magnetic aromaticity in **4** than in **3** (Table 1).

At the same level of calculation, however, another minimum of **4** with a C_1 symmetry is found on the triplet spin state PES, 5.2 kcal·mol^{-1} more stable than the above D_{3d} singlet spin state structure. The σ_r(d) and σ_s(d) values of 0.081 and 0.090 Å, respectively, are larger than those of the singlet spin state

(19) (a) Stanger, A. *J. Org. Chem.* **2006**, *71*, 883. (b) Stanger, A. *Chem. Eur. J.* **2006**, *12*, 2745.

(20) Fallah-Bagher-Shaidaei, H.; Wannere, C. S.; Corminboeuf, C.; Puchta, R.; Schleyer, P. v. R. *Org. Lett.* **2006**, *8*, 863.

(21) In the anionic *carbo*-[3]radialenic series, however, perethynyl susbtitution was shown to result in the reversal of the ring current character, which turns from paratropic (NICS(0) = +4.0 ppm) to strongly diatropic (NICS(0) = −16.4 ppm): Lepetit, C.; Nielsen, M. B.; Diederich, F.; Chauvin, R. *Chem. Eur. J.* **2003**, *9*, 5056.

(22) Fokin, A. A.; Jiao, H.; Schleyer, P. v. R. *J. Am. Chem. Soc.* **1998**, *120*, 9364.

(23) (a) Wei, X.-W.; Darwish, A. D.; Boltalina, O. V.; Hitchcock, P. B.; Street, J. M.; Taylor, R. *Angew. Chem., Int. Ed.* **2001**, *40*, 2989. (b) Darwish, A. D.; Kuvytchko, I. V.; Wei, X.-W.; Boltalina, O. V.; Gol'dt, I. B.; Street, J. M.; Taylor, R. *J. Chem. Soc., Perkin Trans. 2* **2002**, 1118. (c) Burley, G. A.; Avent, A. G.; Boltalina, O. V.; Gol'dt, I. B.; Guldi, D. M.; Marcaccio, M.; Paolucci, F.; Paolucci, D.; Taylor, R. *Chem. Commun.* **2003**, 143. (d) Clare, B. W.; Kepert, D. L.; Taylor, R. *Org. Biomol. Chem.* **2003**, *1*, 3618. (e) Troshin, P. A.; Lyubovskaya, R. N.; Ioffe, I. N.; Shustova, N. B.; Kemnitz, E.; Troyanov, S. I. *Angew. Chem., Int. Ed.* **2005**, *44*, 234.

(24) (a) Havenith, R. W. A.; Rassat, A.; Fowler, P. W. *J. Chem. Soc., Perkin Trans. 2* **2002**, 723. (b) Burley, G. A.; Fowler, P. W.; Soncini, A.; Sandall, J. P. B.; Taylor, R. *Chem. Commun.* **2003**, 3042. (c) Burley, G. A.; Avent, A. G.; Gol'dt, I. B.; Hitchcock, P. B.; Al-Matar, H.; Paolucci, F.; Paolucci, D.; Fowler, P. W.; Soncini, A.; Taylor, R. *Org. Biomol. Chem.* **2004**, *2*, 319.

trannulenic and annulenic forms (Table 1) and are therefore indicative of a lower electron delocalization. The spin density is spread all over the structure, which is highly distorted as compared to the above-described singlet spin state structure. Whatever is the spin state, however, the *carbo*-trannulenic structures are very likely too instable (ca. 60 kcal·mol^{-1} above the *carbo*-annulenic form) to be experimentally isolated. Nevertheless, the symmetrical singlet structure was considered as a brick for the design of new carbon nanotubes (vide infra).

Expanded Carbon Nanotube from *carbo*-[6]Trannulene. Beside those of molecular species, *carbo*-mers of infinite networks may also be envisioned. In particular, *carbo*-mers of all-carbon materials afford novel carbon allotropes. In one dimension, cyclo[3*N*]carbons are the *carbo*-mers of cyclo[*N*]-carbons, and the fictitious carbyne allotrope is its own *carbo*-mer.[25] In two dimensions, the *carbo*-mer of graphite, called 18,18,18-graphyne or α-graphyne, was originally studied at the MNDO-SFC level[26] and more recently at a higher level.[27] Very recently, the corresponding "graphyne nanotube" (α-GNT) has been studied at the DFT level using the PBE functional.[28] In three dimensions, Diederich et al. proposed early that butadiyn-diyl expansion (namely, second *carbo*-merization) of diamond should afford "super diamond".[29] Houk et al. reported on DFT and MM calculations on the second *carbo*-mers of polyhedranes, and very recently, the study was extensively resumed by Bachrach et al.[30] The consideration of the second *carbo*-merization was based on the wealth of copper-catalyzed methods for achieving selective dehydrogenative coupling (dehydrocoupling) of terminal alkynes: 2 R−C≡C−H + 1/2 O_2 → R−C≡C−C≡C−R + H_2O.[31] Although dehydrocoupling of arenes would be more problematic, 2-D carbon allotropes can be formally regarded as total dehydrocoupling products of benzene with various primitive motifs: dehydrobenzene (→ graphene), dehydro-[5]phenylene (→ archimedene),[32] or dehydro-[6]phenylene.[33] Carbon nanotubes can then be devised by wrapping ribbons of planar carbon allotropes; different graphene wrapping processes thus lead to classical single-walled nanotubes of either types: armchair (*n*,*n*), zigzag (*n*,0), or chiral (*n*,*m*) ($m \neq 0$, n).[34]

As an alternative to the "wrapping approach", a "stacking approach" based on the dehydrocoupling process is here considered. It is illustrated here for zigzag nanotubes (Scheme 2).[35] The elementary units of zigzag (*n*,0) nanotubes having the same point symmetry (D_{nh}) as the infinite nanotube are [*n*]cyclacene belts, which are stacked by formal dehydrocoupling. Each belt is built by formal head-to-head dehydrocoupling of two [2*n*]trannulenes of D_{nd} symmetry.[36] [6]Trannulene does not exist, and the corresponding zigzag (3,0) nanotube (of estimated diameter 3.30 Å) does not exist either.[37] By contrast, [18]trannulene is a viable molecule, and the corresponding zigzag (9,0) nanotube does exist as well. Its calculated diameter (using the approximate formula $d = 0.777\ (n^2 + m^2 + nm)^{1/2}$ Å) is equal to 6.99 Å and is thus compatible with buckyball capping (of diameter 6.78 Å) with a minimum deformation.[38]

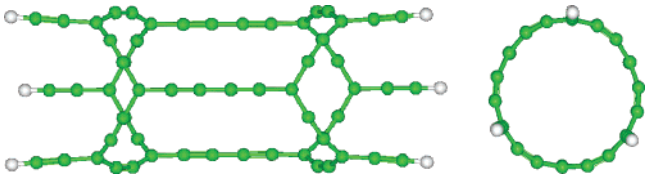

FIGURE 2. Geometry of the hexaethynyl $C_{60}H_6$ segment model **5A** optimized at the B3PW91/6-31G** level in the singlet spin state.

Step 1: The $C_{60}H_6$ Brick, a Model for the C_{60} Unitary Segment. From the above viewpoint, we first envisionned the *carbo*$_{1,2}$-cyclacene **5A** (Scheme 2) built by formal head-to-head dehydrocoupling of two hexaethynyl-*carbo*-[6]trannulene units. The structure of **5A**, calculated at the B3PW91/6-31G** level in the singlet spin state, is a minimum on the PES with a near cylindrical shape of quasi D_{3h} symmetry and a total height of about 18 Å. The apertures of the cylinder are made of three slightly tilted out ethynyl arms (Figure 2).

Structural analysis showed that the C_{18} *carbo*-trannulenic belts of **5A** preserve the in-plane aromaticity characters of the starting *carbo*-trannulene **4**.

The NICS value of −15.0 ppm, computed at the geometric center of the C_{18} *carbo*-trannulene ring of **5A**, is very close to that of hexaethynyl-*carbo*-[6]trannulene **4**, whereas at the geometric center of the cage, NICS is equal to −6.1 ppm. Both values indicate that the overall ring current is of diatropic nature.

A noticeable feature is the existence of a competing triplet state of quasi C_{2v} symmetry lying only 0.85 kcal·mol^{-1} above the corresponding singlet spin state of **5A**. This shows that the algebraic triplet−singlet energy gap increases upon dehydro-stacking of hexaethynyl *carbo*-[6]trannulene units (this energy gap is −5.2 kcal·mol^{-1} in **4**). In the open-shell structure of **5A**, two ethynyl substituents, facing from the opposite apertures, are tilted out from the tube axis. Mulliken spin density analysis indicates that the unpaired electrons are located near these aperture deformations and mainly at the distorted sp^2 carbon atoms, where the spin density mounts to 0.55.

Sequential dehydrocoupling of $C_{60}H_6$ segments **5A** to infinity generates the envisioned nanotube, which is therefore a polymer of C_{60} monomers. However, the π-bonding in the infinite nantotube is actually described by a superimposition of two "orthogonal" resonance structures: the C_{18} belts are either *carbo*-[6]trannulenes connected through butadiyn-diyl rods or

(25) Szafert, S.; Gladysz, J. A. *Chem. Rev.* **2003**, *103*, 4175 and references therein.
(26) Baughman, R. H.; Eckhardt, H.; Kertesz, M. *J. Chem. Phys.* **1987**, *87*, 6687.
(27) Coluci, V. R.; Braga, S. F.; Legoas, S. B.; Galvao, D. S.; Baughman, R. H. *Phys. Rev. B* **2003**, *68*, 035430.
(28) Coluci, V. R.; Braga, S. F.; Legoas, S. B.; Galvao, D. S.; Baughman, R. H. *Nanotechnology* **2004**, *15*, S142.
(29) Diederich, F.; Rubin, Y. *Angew. Chem., Int. Ed. Engl.* **1992**, *31*, 1101.
(30) (a) Jarowski, P. D.; Diederich, F.; Houk, K. N. *J. Org. Chem.* **2005**, *70*, 1671. (b) Bachrach, S. M.; Demoin, D. W. *J. Org. Chem.* **2006**, *71*, 5105.
(31) Fomina, L.; Vazquez, B.; Tkatchouk, E.; Fomine, S. *Tetrahedron* **2002**, *58*, 6741.
(32) (a) De la Vaissière, B.; Fowler, P. W.; Deza, M. *J. Chem. Inf. Comput. Sci.* **2001**, *41*, 376. (b) Bruns, D.; Miura, H.; Vollhardt, K. P. C.; Stanger, A. *Org. Lett.* **2003**, *5*, 549.
(33) Eickmeier, C.; Junga, H.; Matzger, A. J.; Scherhag, F.; Shim, M.; Vollhardt, K. P. C. *Angew. Chem., Int. Ed. Engl.* **1997**, *36*, 2103.
(34) (a) Kornilov, M. Yu. *Dokl. Akad. Nauk UkSSR B* **1977**, *12*, 1097. (b) Kornilov, M. Yu. *Chem. Life*, **1985**, *8*, 22. (c) Ciraci, S.; Dag, S.; Yildirim, T.; Gulseren, O.; Senger, R. T. *J. Phys.: Condens. Matter* **2004**, *16*, R901. (d) Qian, D.; Wagner, G. J.; Liu, W. K.; Yu, M.-F.; Ruoff, R. S. *Appl. Mech. Rev.* **2002**, *55*, 495.
(35) Bulusheva, L. G.; Okotrub, A. V.; Romanov, D. A.; Tomanek, D. *J. Phys. Chem.* A **1998**, *102*, 975.
(36) Choi, H. S.; Kim, K. S. *Angew. Chem., Int. Ed.* **1999**, *38*, 2256.
(37) Mao, Y. L.; Yan, X. H.; Xiao, Y.; Xiang, J.; Yang, Y. R.; Yu, H. L. *Nanotechnology* **2004**, *15*, 1000.
(38) Weber, S. *Crystallography Picture Book*; http://www.jcrystal.com/steffenweber/pb/swpb1.pdf.

SCHEME 3. Resonance Forms of Expanded Carbon Nanotube and Their Finite Analogs

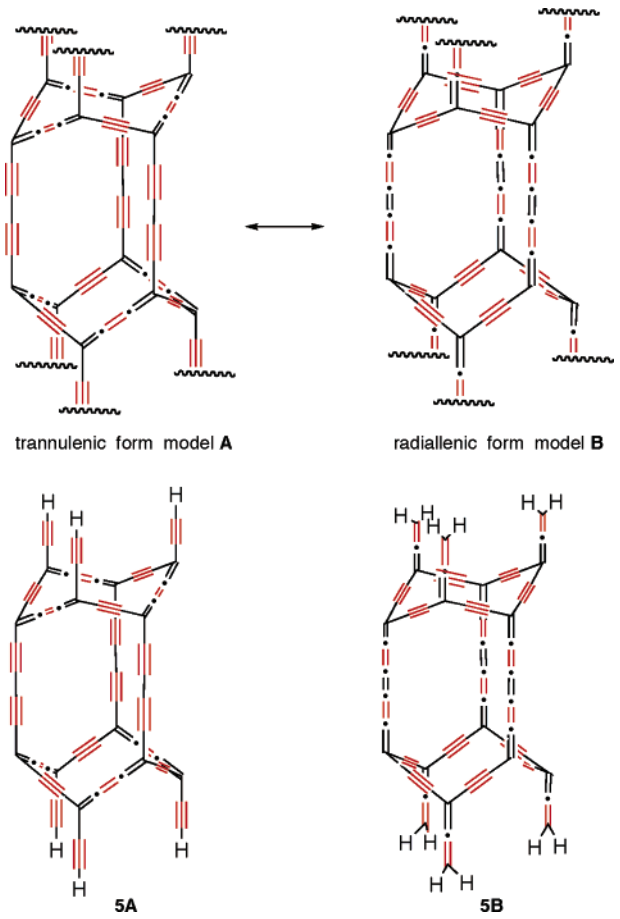

carbo-[6] "radiallenes"[39] connected through butatrien-diylidene rods (Scheme 3). The *local* model for the *carbo*-trannulenic resonance form **A** of the infinite tube is **5A**, with six ethynyl termini, and the *local* model for the *carbo*-radiallenic resonance form **B** is **5B**, with six vinylidene termini- (notice that **5A** and **5B** are neither mesomeric nor even isomeric).

The barrel of the structure **5B** is much more bowed out than that of **5A** (Figure 3). The height of the **5B** cylinder is about

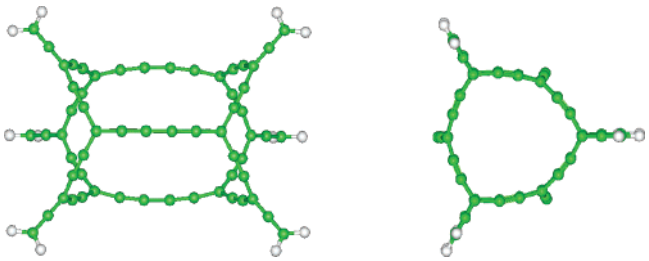

FIGURE 3. Geometry of the hexaallenylidene $C_{60}H_{12}$ segment model **5B** optimized at the B3PW91/6-31G** level in the singlet spin state.

15 Å long, thus shorter than that of **5A.** Whereas the ethynyl termini of **5A** are almost perfectly parallel (cylindrical aperture), the vinylidene termini of **5B** are markedly tilted out of the cage axis (conical aperture). Moreover, whereas the section of **5A** is almost perfectly circular, the section of **5B** is a rounded triangle

(39) By contrast to *carbo*-radialenes, the exocyclic double bonds are cumulated.

TABLE 2. Variation of Sectional and Axial Electron Delocalization upon Increasing the Length of the Nanotube Model (4 → 5A → 6), as Measured by the Mean Bond Length and the Corresponding rms Deviation in the C_{18} Rings (18 Bonds) and in the C_3 or C_6 Rods (2 or 5 Bonds)[a]

	4	5A	6
sectional: $\langle d\rangle_{ring}/\sigma_{ring}(d)$	1.337/0.070	1.339/0.073	1.342/0.077
axial: $\langle d\rangle_{rod}/\sigma_{rod}(d)$	1.317/0.105	1.322/0.080	1.319/0.076

[a] Data are in Å.

(Figure 3). It is also noteworthy that no triplet spin state minimum of **5B** could be obtained.[40]

In conclusion, Figure 3 indicates that the stacking of *carbo*-radiallenic segments **5B** through dehydrocoupling will require much more deformation of the apertures than the stacking of *carbo*-trannulenic segments **5A**.

Step 2: The $(C_{60})_2H_6$ Brick, a Model for the Expanded Zigzag Nanotube. The dehydrocoupling product of two $C_{60}H_6$ segments **5A** affords the $(C_{60})_2H_6$ tubular molecule **6**, which is hereafter theoretically considered. The central C_{60} part of **6** is assumed to be a relevant model for the infinite nanotube. Experimentally, a C_{120} molecule was crystallized as the [2 + 2] dimer of the C_{60} fullerene[41] or its dianion.[42] There are 24 stable isomers in the generalized Stone−Wales fusion pathway to go from the [2 + 2] dimer of the C_{60} fullerene to the completely coalesced C_{120} nanotube.[43] Among them, the vibrational analysis of a stable peanut-shaped C_{120} isomer was described.[44]

In the singlet spin state, the structure of **6** calculated at the B3PW91/6-31G** level is almost perfectly cylindrical (quasi D_{3h}), with a total height of 35.2 Å, and a diameter of 6.7 Å, close to that of the zigzag (9,0) nanotube (Figure 4).[38]

The electron delocalization can be analyzed by comparing the rms bond length deviation inside relevant parts of the tube (Table 2): the zigzag C_{18} rings for the sectional delocalization ($\sigma_{ring}(d)$) and the C_6 rods for the axial delocalization ($\sigma_{rod}(d)$). It is observed that $\sigma_{rod}(d)$ decreases from 0.080 Å in **5A** to 0.076 Å in **6**, while $\sigma_{ring}(d)$ increases from 0.073 Å in **5A** to 0.077 Å in **6**. Therefore, the longer the tube, the stronger the axial delocalization, the weaker the sectional delocalization, and axial and sectional delocalizations converge to the same value in **6**, namely, the original average value: $1/2(0.080 + 0.073) \approx 0.077$ Å (Table 2).

On the basis of this structural criterion, the relative weights of the *carbo*-trannulenic (featuring sectional delocalization) and *carbo*-radiallenic (featuring axial delocalization) resonance forms of **6** (see Scheme 3) are therefore 50:50. Since π and σ MOs are easily distinguished, this resonance weighting can also be visualized through π MO analysis. In particular the lowest π MO is uniformly allocated over sectional C_{18} rings and axial C_6 rods (Figure 5). The HOMO and the LUMO are also delocalized over both rings and rods.

(40) Only one order saddle point (one imaginary frequency of −28.3 cm^{-1}), 12.7 kcal·mol^{-1} higher in energy than the single spin state structure, could be obtained on the triplet spin state PES of **5B**.

(41) Wang, G.-W.; Komatsu, K.; Murata, Y.; Shiro, M. *Nature* **1997**, *387*, 583.

(42) (a) Honnerscheid, A.; Dinnebier, R. E.; Jansen, M. *Acta Crystallogr., B: Struct. Sci.* **2002**, *58*, 482. (b) Konarev, D. V.; Khasanov, S. S.; Otsuka, A.; Saito, G. (c) Konarev, D. V.; Khasanov, S. S.; Saito, G.; Otsuka, A.; Yoshida, Y.; Lyuboskaya, R. N. *J. Am. Chem. Soc.* **2003**, *125*, 10074.

(43) Ueno, H.; Osawa, S.; Takeuchi, K. *Fullerene Sci. Technol.* **1998**, *6*, 319.

(44) Hara, T.; Onoe, J. *Eur. Phys. J. D* **2003**, *24*, 389.

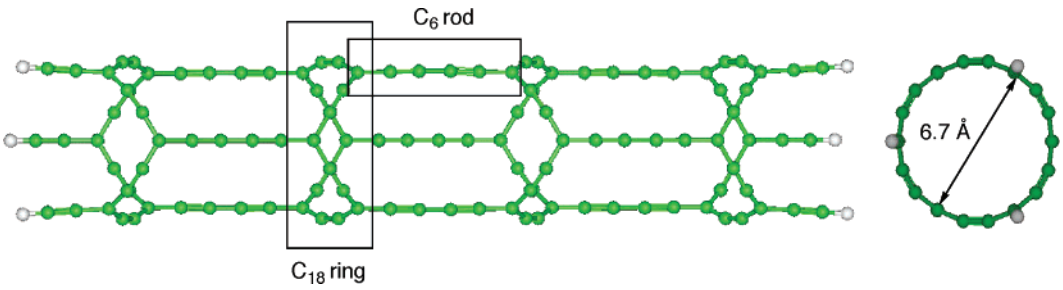

FIGURE 4. Geometry of the $(C_{60})_2H_6$ carbon nanotube model **6** optimized at the B3PW91/6-31G** level in the singlet spin state.

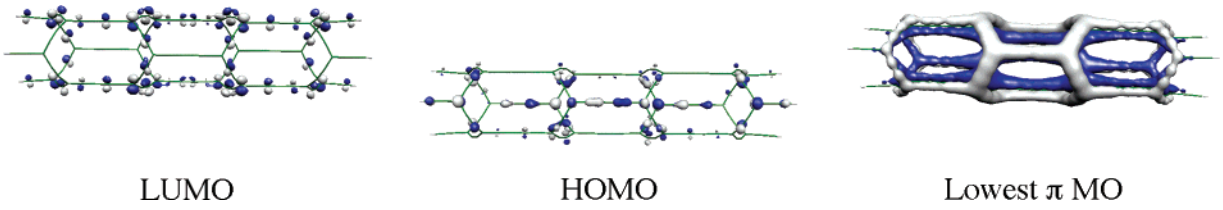

FIGURE 5. Lowest and frontier π orbitals of the singlet nanotube model **6**.

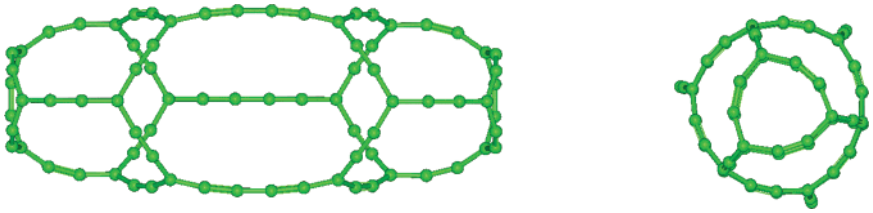

FIGURE 6. Side and top view of the geometry of the C_{78} carbon nanotube model **7**, optimized at the B3PW91/6-31G** level in the singlet spin state.

The HOMO−LUMO gap E_g of the tube model **6** is 0.89 eV. Since hybrid DFT methods are known to shrink this gap, this value is underestimated. As could be anticipated from the extension of the conjugation, E_g(**6**) is however twice smaller than the corresponding HOMO−LUMO gap in the unitary $C_{60}H_x$ ($x = 6$ or 12) segments **5A** (1.43 eV) and **5B** (1.74 eV) and much smaller than the HOMO−LUMO gap in the D_{3d} hexaethynyl-*carbo*[6]trannulene **4** (2.17 eV). Upon further increase of the tube length, the MO diagram will densify to a band diagram, and the HOMO−LUMO gap should diminish toward a band gap smaller than 1 eV. Nonetheless, it is not possible at this stage to ascertain whether the infinite zigzag nanotube *in the singlet state* will be metallic (as predicted for any classical (3*n*,0) zigzag nanotube)[45] or just semiconducting. This ambiguity prompted us to consider the triplet state of the nanotube model **6**.

The triplet spin state of **6** calculated at the UB3PW91/6-31G** level is more stable by 3.2 kcal·mol^{-1} than the corresponding singlet spin state. The quasi-D_{3h} symmetry of the singlet spin state is lost and the ethynyl termini are again tilted out of the tube axis as in the case of the triplet spin state of **5A**. The spin density is spread all over the carbon atoms but especially concentrates on the termini. The latter findings prompted us to consider a capped pure carbon nanotube. In addition, nanotube capping should be required to prevent rearrangement of the H-terminated fragments to fullerenes.[46]

TABLE 3. Comparison of Sectional and Axial Electron Delocalization of Models 5B and 7 as Measured by the Mean Bond Length and the Corresponding rms Deviation in the C_{18} Rings (18 Bonds) and in the C_3 or C_6 Rods (2 or 5 Bonds)[a]

	7	**5B**
sectional: $\langle d\rangle_{ring}/\sigma_{ring}$(d)	1.353/0.091	1.424/0.099
axial: $\langle d\rangle_{rod}/\sigma_{rod}$(d)	1.306/0.047	1.306/0.043

[a] Data are in Å.

A C_{78} unit was built by capping the C_{60} unit of **5A** by two C_9 rings (the isomeric C_{78} fullerene was isolated as a black powder several years ago).[47] The corresponding structure (**7**) was calculated at the B3PW91/6-31G** level in the singlet and triplet spin state. The singlet spin state structure (Figure 6) is now more stable by 7.3 kcal·mol^{-1} than the corresponding triplet state structure. Capping of **5A** thus increases the triplet−singlet energy gap by ca. 6 kcal·mol^{-1}.

The main Lewis structure of **7**, if not zwitterionic, contains cumulenic rods. It must therefore be compared with the *carbo*-radiallenic open reference **5B** (Table 3).

For the open carbon nanotube model **6**, the axial and sectional electron delocalizations were close together (Table 2). By

(45) (a) Mintmire, J. W.; Dunlap, B. I.; White, C. T.; *Phys. Rev. Lett.* **1992**, *68*, 631. (b) Hamada, N.; Sawada, S.; Oshimaya, A. *Phys. Rev. Lett.* **1992**, *68*, 1579. (c) Saito, R.; Fujoita, M.; Dresselhaus, G.; Dresselhaus, M. S. *Phys. Rev. B.* **1992**, *46*, 1804.

(46) (a) Rubin, Y.; Parker, T. C.; Khan, S. I.; Holliman, C. L.; McElvany, S. W. *J. Am. Chem. Soc*. **1996**, *118*, 5308. (b) Tobe, Y.; Nakagawa, N.; Naemura, K.; Wakabayashi, T.; Shida, T.; Achiba, Y. *J. Am. Chem. Soc*. **1998**, *120*, 4544. (c) Tobe, Y.; Umeda, R.; Sonoda, M.; Wakabayashi, T. *Chem. Eur. J.* **2005**, *11*, 1603.

(47) (a) Diederich, F.; Whetten, R. L.; Thilgen, C.; Ettl, R.; Chao, I.; Alvarez, M. M. *Science* **1991**, *254*, 1768. (b) Kikuchi, K.; Nakahara, N.; Wakabayashi, T.; Suzuki, S.; Shiromaru, H.; Miyake, Y.; Saito, K.; Ikemoto, I.; Kainosho, M.; Achiba, Y. *Nature* **1992**, *357*, 142.

TABLE 4. Cohesive Energy E_{coh} (in eV) for the Various Nanotubes Models Estimated at the B3PW91/6-31G* Level

compound	E_{coh} (ZPE corr)[a]
7: C_{78}	7.08
6: $C_{120}H_6$ singlet	6.55
6: $C_{120}H_6$ triplet	6.56
5A: $C_{60}H_6$	6.66 (6.50)
5B: $C_{60}H_{12}$	8.40 (8.20)

[a] Values in parentheses are corrected from the zero-point energy (ZPE).

contrast, in model **7**, as in model **5B** (Table 3), the axial electron delocalization is much higher than the sectional one. However, the effect of capping is stronger on the sectional electron delocalization than on the axial one.[48]

The stability of carbon nanotubes is generally estimated through the cohesive energy E_{coh}, namely, the negative of the heat of formation per carbon atom. To compare the stability of the partially hydrogenated nanotube models **5**−**7**, a generalized cohesive energy definition, applicable to molecular systems, is proposed here for any hydrogenated nanotube model **x**:

$$E_{coh}(\mathbf{x}) = 1/n\{nE[\mathrm{C}] + 6E[\mathrm{H}] - E_{Total}[\mathbf{x}]\}$$

where E[C] and E[H] stand for the energy of an isolated carbon atom or hydrogen atom, respectively, and n is the number of carbon atoms in the model. The cohesive energy values calculated for nanotube models **5**−**7** are given in Table 4. The ZPE correction, which was only available for the smaller models **5A,B**, decreases the values very slightly. These cohesive energies are generally lower than the reported experimental cohesive energy of graphene, 7.34 eV,[49] and lie in the range of cohesive energies of graphene calculated at the LDA level (7−10 eV).[50] The capped nanotube model **7** appears to be the most stable model considered in this work (apart from model **5B**, which contains 12 hydrogen atoms and which is not suitable for the construction of infinite nanotubes). The two last rows of Table 4 illustrate that the cohesive energy varies with the C/H ratio, at least for short nanotube models; model **7** is therefore the first member of a new familly of viable carbon nanotubes.

(48) The influence of the lengthening of the model on this cap effect and on the restoration of the electron delocalization will be further studied.

(49) Yin, M. T.; Cohen, M. L. *Phys. Rev. B* **1984**, *29*, 6996.

(50) (a) Dunlap, B. I.; Boettger, J. C. *J. Phys. B: At., Mol. Opt. Phys.* **1996**, *29*, 4907. (b) Kurti, J.; Zolyomi, V.; Kertesz, M.; Sun, G.; Baughman, R. H.; Kuzmany, H. *Carbon* **2004**, *42*, 971.

Conclusion

Beyond its aestetic and academic interest, the novel carbon nanotube structure would require solving practical problems and in particular the capping problem. Although a few uncapped carbon nanotubes are known, most of them are indeed capped.[51] According to the rule governing the structure of fullerenes, the caps of sufficiently large nanotubes derived from graphene must contain six nonadjacent pentagons. Because of the restricted 3-fold symmetry of the aperture of our expanded nanotube, the classical buckyball caps fitting the C_{18} circumference of (9,0) zigzag nanotubes are here precluded. One thus resorted to a C_9 trigonal prism made of six sp and three sp^2 carbons. In a model approach, it might also be envisoned to use a C_7 bowed pyramidal cap with a sp^3 carbon vertex saturated by a hydrogen or fluorine terminal atom.[52]

In a further outlook, the proposed expanded carbon nanotube naturally meets more applied concerns such as electrical, optical, or mechanical properties on the one hand and storage or sensor chemical properties on the other hand. Within this latter respect, the most exciting feature of an expanded carbon nanotube is the sidewall porosity, which would facilitate endohedral doping. Of course, beyond the $(C_{60})_2H_6$ model, further studies are required to accurately establish the stability and conducting properties of the infinite nanotube. Nevertheless, these preliminary results encourage long term experimental efforts, which are currently in progress in our group.

Acknowledgment. The authors would like to thank Dr. Jean-Louis Heully for fruitful discussions, CALMIP (Calcul intensif en Midi-Pyrénées,Toulouse, France), IDRIS (Institut du Développement et des Ressources en Informatique Scientifique, Orsay, France) and CINES (Centre Informatique de l'Enseignement Supérieur, Montpellier, France) for computing facilities and the Ministère de l'Education Nationale de la Recherche et de la Technologie for ACI financial support.

Supporting Information Available: Cartesian coordinates, total electronic energies in hartrees, symmetry and number of imaginary frequencies (NImag) of structures **1**−**4**, **5A,B**, **6**, and **7** computed at the B3PW91/6-31G** level. This material is available free of charge via the Internet at http://pubs.acs.org.

JO052551J

(51) Stobinski, L.; Peszke, J.; Lin, H.-M. *Rev. Adv. Mater. Sci.* **2003**, *5*, 363.

(52) Stojkovic, D.; Zhang, P.; Crespi, V. H. *Phys. Rev. Lett.* **2001**, *87*, 125502−1.